JACS
JOURNAL OF THE AMERICAN CHEMICAL SOCIETY

Article

pubs.acs.org/JACS

Defining Rules for the Shape Evolution of Gold Nanoparticles

Mark R. Langille,[†] Michelle L. Personick,[†] Jian Zhang,[‡] and Chad A. Mirkin*

Department of Chemistry and International Institute for Nanotechnology, Northwestern University, 2145 Sheridan Road, Evanston, Illinois 60208, United States

Supporting Information

ABSTRACT: The roles of silver ions and halides (chloride, bromide, and iodide) in the seed-mediated synthesis of gold nanostructures have been investigated, and their influence on the growth of 10 classes of nanoparticles that differ in shape has been determined. We systematically studied the effects that each chemical component has on the particle shape, on the rate of particle formation, and on the chemical composition of the particle surface. We demonstrate that halides can be used to (1) adjust the reduction potential of the gold ion species in solution and (2) passivate the gold nanoparticle surface, both of which control the reaction kinetics and thus enable the selective synthesis of a series of different particle shapes. We also show that silver ions can be used as an underpotential deposition agent to access a different set of particle shapes by controlling growth of the resulting gold nanoparticles through surface passivation (more so than kinetic effects). Importantly, we show that the density of silver coverage can be controlled by the amount and type of halide present in solution. This behavior arises from the decreasing stability of the underpotentially deposited silver layer in the presence of larger halides due to the relative strengths of the Ag^{+}/Ag^{0}–halide and Au^{+}/Au^{0}–halide interactions, as well as the passivation effects of the halides on the gold particle surface. We summarize this work by proposing a set of design considerations for controlling the growth and final shape of gold nanoparticles prepared by seed-mediated syntheses through the judicious use of halides and silver ions.

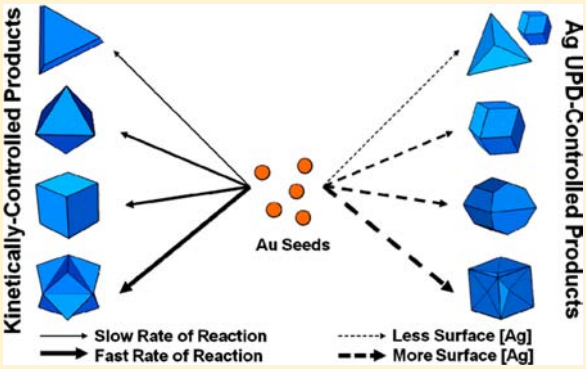

INTRODUCTION

Anisotropic noble metal nanoparticles have attracted a great deal of attention and research effort due to their shape- and size-dependent physical and chemical properties. These properties have led to the development of numerous applications in areas such as spectroscopy,[1−8] catalysis,[9,10] energy,[11] and biology.[12] However, to take full advantage of the unique physical and chemical attributes of these nanostructures, it is necessary to have synthetic methods for rationally controlling their size, shape, and composition.[9,13] Of these characteristics, shape has proven to be one of the most challenging to deliberately control, yet it is arguably among the most useful parameters for tailoring the properties of a nanoparticle, particularly for particles comprised of gold. One of the most versatile methods for generating gold nanoparticles of a desired shape is the thermal seed-mediated synthesis,[14−16] which has led to the production of a vast library of nanostructures, ranging from Platonic solids such as octahedra and cubes,[15,17−19] to plates and prisms,[3,4,20,21] to more exotic structures with high-index surface facets.[22−25] It is acknowledged in the literature that additives, most commonly halides and silver ions, play a key role in directing the growth of anisotropic nanostructures in this synthetic method.[21,23,26−30] For example, we have previously reported that low, but detectable, concentrations of iodide impurities present in a bromide-containing surfactant significantly affect particle growth, with reactions yielding gold spheres, rods, or triangular prisms with increasing concentrations of iodide ions due to the binding of iodide to the gold nanoparticle surface.[21] In addition, silver ions are a particularly interesting additive, because a number of reports have observed the growth and stabilization of gold nanostructures bound by high-index facets due to their presence,[22−24,30,31] and these nanostructures are of potential use for catalytic applications due to the high number of low-coordinated surface atoms exposed on such facets.[32,33] We have recently studied the role of silver ions in the seed-mediated synthesis for a series of reactions conducted with a chloride-containing surfactant.[26] It was determined that through the underpotential deposition of a near-monolayer of silver onto the surface of the gold nanoparticles, judicious control of the silver ion concentration in the growth solution allowed for the selective preparation of a variety of gold nanostructures, including {110}-faceted rhombic dodecahedra and bipyramids,[34] {310}-faceted truncated ditetragonal prisms,[26] {720}-faceted concave cubes,[24] and {111}-faceted octahedra with tailorable hollow features.[35] However, the role of chloride ions in these syntheses has, until now, not been addressed and a consistent explanation for the role of the other commonly used halides, namely bromide and iodide, in the seed-mediated synthesis in either the absence or presence of silver ions is still lacking. In the

Received: June 1, 2012
Published: August 24, 2012

   dx.doi.org/10.1021/ja305245g | J. Am. Chem. Soc. 2012, 134, 14542−14554

following article, we discuss the results of a detailed study designed to elucidate the independent and synergistic effects of silver ion and the halides (chloride, bromide, and iodide) on the growth of anisotropic nanostructures, with a focus on explaining how these chemical components can act together to affect reaction kinetics and surface silver coverage to yield gold nanostructures of a particular morphology. On the basis of this study, we also provide a series of generally applicable design parameters for the directed synthesis of gold nanoparticles in the seed-mediated method through the controlled use of halides and silver ions.

A number of diverse and, at times, conflicting theories exist to explain the role of halides in the seed-mediated synthesis, in both the absence and presence of silver ions. The most widespread explanation for the role of bromide anions is that they bind to {100}-faceted surfaces, stabilizing those surfaces and slowing gold deposition at that site, thus leading to the formation of {100}-faceted nanoparticles, such as cubes.[15,25,36,37] However, other proposed explanations include the selective binding of bromide to {110} or {111} surfaces[16,27,29] or formation of cetyltrimethylammonium bromide (CTA-Br) micelles, bilayers, or CTA-Au-Br complexes that physically template nanorod formation or slow the rate of gold deposition.[16,29,37,38] In the presence of silver ions, bromide has been proposed to lead to the formation of silver bromide (or CTA-Ag-Br), which deposits selectively onto certain surfaces, through either adsorption[14,27,29,37,39] or underpotential deposition.[23,40,41] For iodide, which has only been investigated more recently, the case is even more complex. Iodide is commonly thought to bind to and stabilize {111} facets,[21,42−45] but some researchers have proposed that it acts as a reducing agent to increase the rate of $[AuCl_4]^-$ reduction.[28,43] However, in other reports iodide is claimed to slow the growth of gold nanoparticles[42]—results which are contradictory. In the presence of silver ions, the effects of iodide on particle growth are proposed to dominate the effects of silver ions.[46] Taken together, iodide has been proposed to (1) bind to the surface with silver ion and form a layer of silver iodide, (2) act as a catalyst for the reduction of gold ions onto {111} surfaces,[44,46] and (3) seed gold nanoparticle growth by acting as a nucleation site.[43] Consequently, there is little convergence and self-consistency among the proposed theories for the role of silver ion and the halides in nanocluster growth. Assuming that bromide and iodide act via similar mechanisms in each variation of the seed-mediated synthesis (the reaction conditions are very similar), it would be useful to determine the role of each additive. Moreover, it would be worthwhile to develop a series of design considerations by which the principles of action of these two anions in the presence and absence of silver ions can be better understood and applied to the syntheses of gold nanoparticles of a desired shape.

One of the most illustrative examples of the use of halides in controlling gold nanoparticle shape is the case of the silver-assisted syntheses of concave cubes[24] and tetrahexahedra,[22] both of which are bound by similar high-index facets. The synthetic conditions for producing these two particles are nearly identical, except that the {720}-faceted concave cubes[24] are synthesized in cetyltrimethylammonium chloride (CTA-Cl), while the same synthesis in the analogous bromide-containing surfactant, cetyltrimethylammonium bromide (CTA-BR), results in convex {730}-faceted tetrahexahedra (Figure 1).[22] These are closely related shapes that are best described as a cube having either square-pyramidal depressions (concave cubes) or square pyramids (tetrahexahedra) on each of the six faces. The reason for this

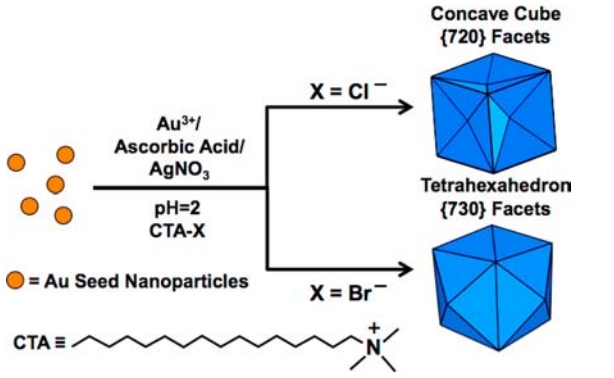

Figure 1. In a seed-mediated synthesis of gold nanoparticles, the use of a silver ion additive in the presence of a chloride-containing surfactant (CTA-Cl) results in the growth of {720}-faceted concave cubes (upper growth pathway), while the use of a bromide-containing surfactant (CTA-Br) under otherwise identical conditions results in the growth of {730}-faceted tetrahexahedra (lower growth pathway).

difference in morphology has, up to this point, not been elucidated. To understand why the growth of concave cubes and tetrahexahedra is favored in chloride- and bromide-containing surfactants, respectively, we have studied the role of halides in the absence of silver ions and the role of silver ions in the presence of two different ranges of halide concentrations. However, our findings are of interest to all particles, regardless of shape, prepared by this synthetic method.

In the following article, we first clarify the role of each of the halides in the absence of silver ions and show that the introduction of bromide or iodide to a growth solution containing a chloride-containing surfactant slows the rate of gold ion reduction and results in particles bound by lower-energy surface facets. We also show that iodide decreases the rate of gold ion reduction more significantly than bromide does. These effects arise from larger, less electronegative halides both forming halide−gold ion complexes with decreasing reduction potentials and having an increasing binding affinity for the gold nanoparticle surface. We summarize previous results involving the control of particle shape by silver underpotential deposition[26] and present new data showing that silver ions also reduce the rate of particle growth by physically and chemically inhibiting the deposition of gold onto the particle surface. X-ray photoelectron spectroscopy (XPS) characterization of the surface of each particle type and inductively coupled plasma atomic emission spectroscopy (ICP-AES) kinetic studies are used to show that, in the presence of a silver ion additive, the addition of a larger halide to a surfactant containing a smaller halide causes a decrease in the stability of the Ag_{UPD} layer (it is more susceptible to surface rearrangement) relative to its stability in the absence of the larger halide. Destabilization of the Ag_{UPD} layer is due to the decreasing binding affinity of larger halides for the Ag_{UPD} layer and is dependent on the concentration of the halide. Consequently, judicious control over the type and amount of halide in solution allows for the relative strengths of the Ag^+/Ag^0−halide and Au^+/Au^0−halide interactions to be tailored, enabling control over the silver coverage and shape of the gold nanoparticles produced. We discuss the implications of these results for understanding the formation of the concave cubes and tetrahexahedra and provide a series of design considerations for the shape-controlled growth of gold nanoparticles prepared by the seed-mediated synthetic approach.

dx.doi.org/10.1021/ja305245g | J. Am. Chem. Soc. 2012, 134, 14542−14554

RESULTS

In a typical seed-mediated synthesis of gold nanoparticles, small seeds (~7 nm diameter) were first prepared by the rapid reduction of $HAuCl_4$ by sodium borohydride in the presence of CTA-Cl, a chloride-containing surfactant. In some instances, larger seeds were desired, and these were obtained by regrowing the ~7 nm diameter seeds in a growth solution containing $HAuCl_4$, CTA-Cl, and ascorbic acid to yield spherical particles with an average diameter of ~40 nm. An aqueous growth solution was then prepared which contained at least the following reagents: $HAuCl_4$, surfactant (either CTA-Cl or CTA-Br), and ascorbic acid. In these reactions, the ascorbic acid reduces Au^{3+} to Au^+ to yield a colorless solution, and the addition of seed particles catalyzes the reduction of Au^+ to Au^0 to generate larger gold particles.[14−16] Au^+ is stabilized against disproportionation by binding to CTA-X to form a stable CTA-X-AuX_2^- complex.[47,48] Experiments were conducted to elucidate the roles of silver ions and halides in controlling the growth and final shape of the resulting nanoparticles. These investigations were carried out by systematically varying the constituents of the growth solutions. Hydrochloric acid was used to control the solution pH, NaBr and NaI were used to introduce Br^- and I^- species, respectively, and $AgNO_3$ was used as the source of Ag^+. The particle size can be controlled by varying the amount of seeds added to the growth solution, with larger amounts of seeds generating many small particles, while smaller amounts of seeds lead to fewer, but larger, particles. However, in the experiments that follow, the volume of seed solution added was held constant across each set of reactions to limit the number of variables. In addition to the experimental details provided in each subsection of the Results and Discussion, a full list of experimental conditions can be found in the Supporting Information (Chart S1).

Effects of Reducing Agent Concentration. The most direct way of controlling the reaction kinetics, and thus particle shape, in these syntheses is by changing the concentration of the reducing agent, ascorbic acid. Increasing the amount of reducing agent in the growth solution increases the rate of gold ion reduction, which should create a preference for the growth of more kinetically favorable (or less thermodynamically favorable) particle morphologies. To understand the role of other additives, such as silver ions and halides, it is important to first fully explain and isolate the effect of ascorbic acid, because it is present in all of the reaction solutions. To establish the role of the reducing agent, growth solutions were prepared which contained 10 mM CTA-Br, 0.125 mM $HAuCl_4$, 500 μL of 40 nm diameter seeds, and either 0.5, 2.0, or 10.0 mM ascorbic acid (Chart S1). Scanning electron microscopy (SEM) images of the products of these reactions reveal that the concentration of reducing agent does indeed have a significant impact on the shape of the product (Figure 2). At 0.5 and 2.0 mM ascorbic acid, the reactions generate well-formed {111}-faceted octahedra (Figure 2A) and {100}-faceted cubes (Figure 2B), respectively. When the concentration of ascorbic acid is increased to 10.0 mM, the products resemble ill-formed trisoctahedra (Figure 2C). These particles are likely bound by high-index facets, as suggested by characterization studies of well-formed trisoctahedra;[49] however, we suspect that these reaction conditions are not ideal for generating such structures and that this particular particle morphology is indicative of poorly controlled growth due to a very rapid rate of gold ion reduction. Nonetheless, these observations indicate that, as the concentration of reducing agent is increased, particles bound by higher-energy surface facets are produced. These results are consistent with many other studies of the use of ascorbic acid in the seed-mediated synthesis.[25,38,50,51]

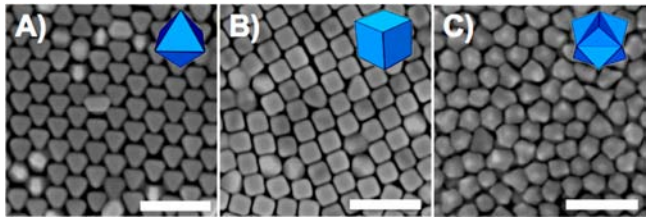

Figure 2. SEM images of reaction products from growth solutions containing 10 mM CTA-Br and (A) 0.5, (B) 2.0, and (C) 10.0 mM ascorbic acid, resulting in the formation of {111}-faceted octahedra, {100}-faceted cubes, and high-index faceted trisoctahedra, respectively. Scale bars: 200 nm.

Effects of Halides in the Absence of Silver Ions. We have determined that, in the absence of silver ions, halides affect particle growth through two separate but cooperative pathways. First, the halides present in solution will complex gold ion species, thereby affecting the reduction potential and solubility of the gold ions in the CTA-X-AuX_2^- complexes and thus changing their reduction rate.[48,51] Indeed, the reduction potentials for Au^+-halide complexes decrease in the order $[AuCl_2]^-$ > $[AuBr_2]^-$ > $[AuI_2]^-$ (1.154 > 0.960 > 0.578 V), meaning that the addition of bromide or iodide to a chloride-containing surfactant will decrease the ability of Au^+ to be reduced by ascorbic acid.[52] The solubilities of the $[AuX_2]^-$ complexes decrease in the same order,[53] and this decreasing solubility relative to the high solubility of CTA-X-AuX_2^- will also slow the rate of gold reduction. Second, the halides can bind to the surface of the gold nanoparticles, inhibiting the subsequent growth of the particles. The binding strength of the halides to an Au particle surface increases in the order $Cl^- < Br^- < I^-$.[54] Thus, the introduction of bromide or iodide will slow the rate of gold nanoparticle formation as compared to the rate in the presence of chloride alone both by lowering the reduction potential and solubility of the gold ion species in solution and by binding strongly to the surface of the gold particles. Note that the relative importance of these separate pathways is difficult to distinguish, but both follow similar trends with respect to affecting the rate of gold deposition, and thus we are able to control particle shape by simply varying the concentrations of different halides in the growth solution. Indeed, when the previous reactions are conducted with the chloride-containing surfactant CTA-Cl rather than the bromide-containing CTA-Br, we can produce trisoctahedra even at low concentrations of ascorbic acid (1.0 mM, Figure 3A). This indicates that the rate of gold ion reduction is more rapid in the presence of CTA-Cl than in CTA-Br, since high-index facets are formed at a comparatively low concentration of reducing agent. To investigate the consequences of bromide anions on particle formation, a growth solution containing 50 mM CTA-Cl and 5.0 mM NaBr was prepared (in addition to 0.5 mM $HAuCl_4$, 1.0 mM ascorbic acid, and 0.1 μL of 7 nm diameter seeds; Chart S1). We note that the concentration of bromide in this solution is much greater than the concentration of gold ion in the reaction. This reaction produced {100}-faceted cubes (Figure 3B), which are the same structures observed when the amount of reducing agent is decreased with a bromide-containing surfactant, consistent with the conclusion that the introduction of bromide into CTA-Cl is reducing the rate of gold ion reduction. To test this theory, ICP-AES was used to monitor the rate of Au^0 production. Samples were taken from the growth solution at specific time

dx.doi.org/10.1021/ja305245g | J. Am. Chem. Soc. 2012, 134, 14542−14554

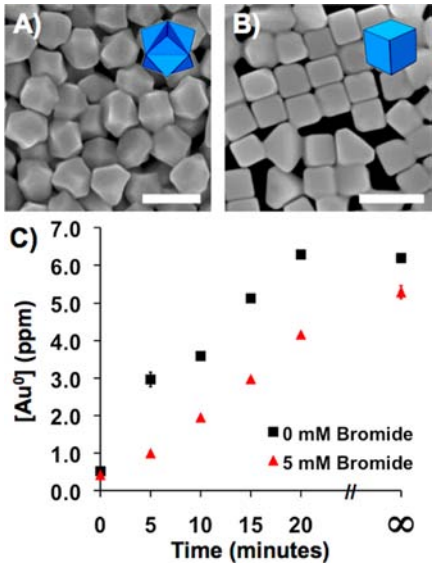

Figure 3. (A, B) SEM images of reaction products from growth solutions containing 50 mM CTA-Cl and (A) 0.0 and (B) 5.0 mM NaBr, resulting in the formation of high-index faceted trisoctahedra and {100}-faceted cubes, respectively. Scale bars: 200 nm. (C) ICP-AES kinetics data of the reactions containing 0.0 mM (black squares) and 5.0 mM (red triangles) NaBr.

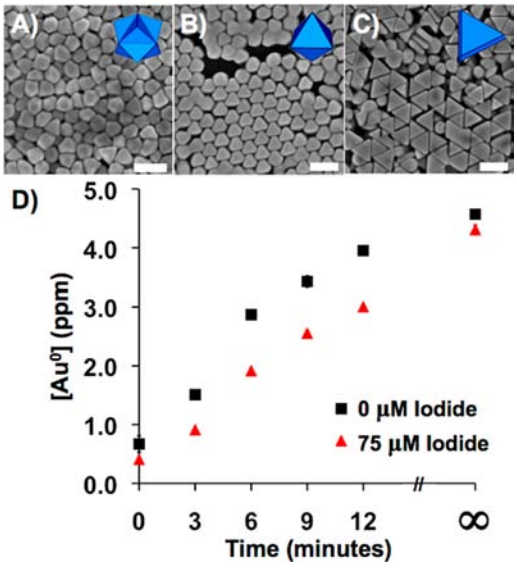

Figure 4. (A–C) SEM images of reaction products from growth solutions containing 50 mM CTA-Cl and (A) 0.0, (B) 10.0, and (C) 75.0 μM NaI, resulting in the formation of high-index faceted trisoctahedra, {111}-faceted octahedra, and {111}-faceted truncated bitetrahedra, respectively. Scale bars: 200 nm. The truncated bitetrahedra are the planar twinned analogue of the single crystalline octahedra. (D) ICP-AES kinetics data of the reactions containing 0.0 μM (black squares) and 75.0 μM (red triangles) NaI.

points during the course of the reaction, and these samples were then quenched using an excess of bis(*p*-sulfonatophenyl)-phenylphosphine dihydrate potassium salt (BSPP), which strongly coordinates to gold ions in solution and to the gold particle surface, thus slowing (inhibiting) the further reduction of gold ions.[55−57] From each sample, the gold particles were isolated by centrifugation, separating them from gold ions in solution, and subsequently dissolved with aqua regia. ICP-AES was then used to determine the total amount of gold in the sample. Note that the addition of seeds to these reactions separates the nucleation from the growth event and thus the amount of Au^0 detected is due to the growth of the seeds and not due to the nucleation of new seed particles. A comparison of the reactions containing 0.0 and 5.0 mM NaBr, which produced trisoctahedra and {100}-faceted cubes, respectively, is shown in Figure 3C. In both sets of data, the amount of Au^0 increases with time due to the formation of gold nanoparticles. However, Au^0 is produced more rapidly for the reaction containing 0.0 mM NaBr than for the reaction containing 5.0 mM NaBr, indicating that the presence of bromide is inhibiting the rate of gold particle formation and, accordingly, the rate of gold ion reduction. We note that {111}-faceted octahedra can also be produced at 5.0−10.0 mM NaBr by slightly lowering the concentration of reducing agent in the reaction solution, indicating that the kinetics of formation of these two products differ only slightly (Figure S1, Supporting Information). This similarity in the rate of particle formation is likely due to {111} and {100} facets of gold being very close in surface energy.[58−60]

A similar trend is observed when iodide is introduced to reactions run in the presence of CTA-Cl. However, iodide can be added to the growth solutions in an amount 2 orders of magnitude lower than is required for bromide while achieving comparable results. Growth solutions containing 0.0, 10.0, and 75.0 μM NaI yield trisoctahedra, {111}-faceted octahedra, and {111}-faceted truncated bitetrahedra, respectively (Figure 4). The ICP-AES data shown in Figure 4D indicate a decrease in the rate of Au^0 generation with the addition of 75.0 μM NaI, confirming that, as with bromide, the addition of iodide to the reaction inhibits the rate of gold ion reduction. Another difference between the examples involving bromide and iodide is that the use of 75.0 μM iodide results in the formation of a planar twinned product, truncated bitetrahedra, while high concentrations of bromide produce cubes, which are single crystalline. Twin planes are a common defect observed in the growth of noble metal nanostructures, and their presence is indicative of slow, kinetically controlled growth conditions.[61−67] The growth of planar twinned truncated bitetrahedra with 75.0 μM NaI is therefore not surprising if iodide is acting to reduce the rate of gold ion reduction. We also do not observe the growth of {100}-faceted cubes when iodide is used; however, the {111}-faceted octahedra do display some tip truncations that expose {100} facets. Again, it is likely that the small difference in energy between {111} and {100} surface facets is the cause for these observations.

As previously mentioned, the two effects of halides on particle growth, namely, on the reduction rates of the gold ion species and on the binding of the halide to the gold particle surface, are difficult to separate. For example, ICP-AES data for the reactions containing 10.0 and 75.0 μM NaI cannot be distinguished (data not shown), indicating that the introduction of iodide affects more than just the rate of reaction, since the formation of both {111}-faceted octahedra and {111}-faceted truncated bitetrahedra appear to have the same rate of gold particle generation yet produce different particle shapes. This indicates that the rate of growth of planar twinned seeds is faster than the rate of growth of the single-crystalline counterparts under the conditions that produce {111}-faceted truncated bitetrahedra, but a comprehensive understanding of how all twinned particles fit into our model of kinetically controlled growth will still need to be determined.

Effects of Silver Ions. In previous work,[26] we demonstrated that particle shape can be controlled by varying the amount of

dx.doi.org/10.1021/ja305245g | J. Am. Chem. Soc. 2012, 134, 14542−14554

silver ion additive in a growth solution containing CTA-Cl surfactant. Silver deposits epitaxially onto gold and prefers to deposit onto sites where it will have a high coordination number with respect to gold, such as kinks and step edges, and this leads to the stabilization of high-index facets through silver acting as a capping layer. By incrementally raising the concentration of silver ion in the growth solution, particles with increasingly higher index facets are formed due to the underpotential deposition of silver onto the surface of the growing gold particle.[26] This corresponds to particles with an increasing number of exposed surface atoms per unit area: {110}-faceted rhombic dodecahedra, {310}-faceted truncated ditetragonal prisms, and {720}-faceted concave cubes, respectively. Note that the {110}-faceted rhombic dodecahedra form concomitantly with their planar twinned analogue, {110}-faceted bipyramids.[34] Using XPS and ICP-AES, we determined that the ratio of silver to gold on the surface of the particles (via XPS), as well as in the particles as a whole (via ICP-AES), increases with greater concentrations of silver ion in the growth solution (Figure 5).[26] This

A)

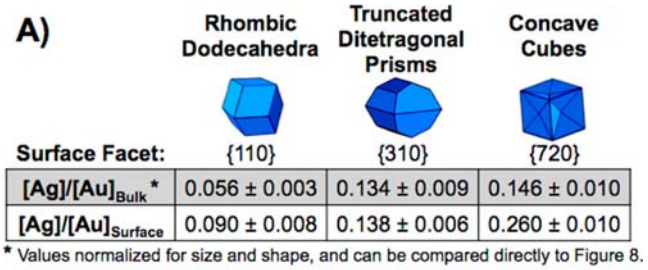

Surface Facet:	{110}	{310}	{720}
$[Ag]/[Au]_{Bulk}$*	0.056 ± 0.003	0.134 ± 0.009	0.146 ± 0.010
$[Ag]/[Au]_{Surface}$	0.090 ± 0.008	0.138 ± 0.006	0.260 ± 0.010

* Values normalized for size and shape, and can be compared directly to Figure 8.

B)

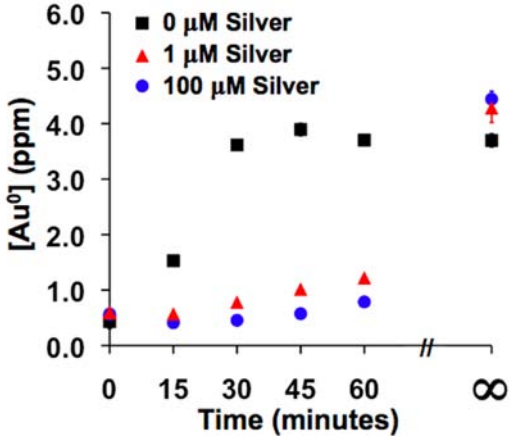

Figure 5. (A) Chart of the silver/gold ratios for {110}-faceted rhombic dodecahedra, {310}-faceted truncated ditetragonal prisms, and {720}-faceted concave cubes as determined by ICP-AES, a bulk characterization technique, and XPS, a surface characterization technique. The silver/gold ratio on the surface of the particles increases in the order rhombic dodecahedra < truncated ditetragonal prisms < concave cubes due to higher-index facets having more open surfaces with more exposed surface sites. Note that the bulk silver/gold ratios determined by ICP-AES are normalized for both the size and shape of the nanoparticles and thus represent a value reflecting the silver coverage on the particle surface. See ref 26 for a more detailed discussion of this adjustment. The $[Ag]/[Au]_{bulk}$ values provided in the table can be directly compared with the ICP-AES data provided in Figure 8. (B) ICP-AES kinetics data of the reactions containing 0 μM (black squares), 1 μM (red triangles), and 100 μM (blue circles) $AgNO_3$.

result matches well with what would be expected for a submonolayer coverage of silver on each of the different facet types. Thus, the data provide quantitative evidence that silver ions control gold nanoparticle growth in the seed-mediated synthesis in the presence of CTA-Cl through underpotential deposition of up to a monolayer of silver onto the facet with the highest number of exposed surface atoms for which there is sufficient silver to cover.[26] Once silver deposits onto a particular facet, it slows further growth of that facet by inhibiting gold deposition, and therefore that facet is retained in the final nanoparticle morphology. To further validate this claim, we showed that by introducing more silver ion than that required to form concave cubes, we were able to selectively stabilize {111} facets to generate octahedra with hollow features, which correlates well with {111} being the most densely packed facet for face-centered cubic gold.[35] In the current study, we are also interested in the effects that the silver ion additive has on the reaction rate, and through an ICP-AES study of the rate of gold nanoparticle formation, we show that increasing amounts of silver ion additive slow the rate of nanoparticle growth (Figure 5). This is in agreement with what we would expect, since silver inhibits gold deposition onto the particles, higher concentrations of silver ions should inhibit gold deposition more effectively. However, we note that the slowed rates of gold particle growth are very similar for substantially different concentrations of silver ions in the growth solution. Note that 1 and 100 μM represent the entire $[Ag^+]$ range studied in our shape-controlled syntheses. This suggests that rather than reaction kinetics being the dominant factor affecting particle growth and shape, as is the case in the absence of silver ions, surface effects are more influential in the case of the Ag^0 underpotential deposition-controlled particle syntheses.

Effects of Trace Halides in the Presence of Silver Ions. The effects of halides on particle growth are more complicated when silver ions are introduced into the reaction because the halides interact not only with the gold ions in solution and the gold nanoparticle surface but also with the silver ions in solution and the Ag_{UPD} layer on the surface of the particles. Fortunately, the effects of halides on the underpotential deposition of silver onto bulk gold surfaces have been studied by others in great detail,[68−72] and while these studies are typically conducted on planar gold surfaces in electrochemical cells, we show here how the same effects explain the behavior of these chemical components in the context of the growth of gold nanoparticles in the seed-mediated synthesis. It has been observed that the presence of a chloride adlayer over an Ag_{UPD} layer results in the formation of the most stable Ag_{UPD} layer in comparison to either bromide or iodide and that adlayers of bromide or iodide lead to Ag_{UPD} layers with decreasing stability.[68−72] This behavior is exemplified in a series of experiments conducted by Michalitsch and Laibinis,[68] where an Ag_{UPD} layer was first electrochemically prepared on a gold surface and then subsequently stripped either in the presence of chloride, bromide, or iodide or in the absence of halides (presence of sulfate ions). The stripping peak in the absence of a halide was found to be at 534 mV, while the peak shifted to 615, 574, or 415 mV in the presence of chloride, bromide, or iodide, respectively.[68] These data indicate that the stability of an Ag_{UPD} layer decreases in the order Cl^- > Br^- > absence of halide > I^-. These results would be expected when considering either enthalpic or solubility arguments. In a simplified view, the formation of an Ag_{UPD} layer can be described as the breaking (or dissociation) of an Au−halide bond accompanied by the formation (or association) of an Ag−halide bond. Whether considering enthalpies of formation or solubility constants, the formation of an Ag_{UPD} layer is more favorable in the presence of halides in the order Cl^- > Br^- > I^-

dx.doi.org/10.1021/ja305245g | J. Am. Chem. Soc. 2012, 134, 14542−14554

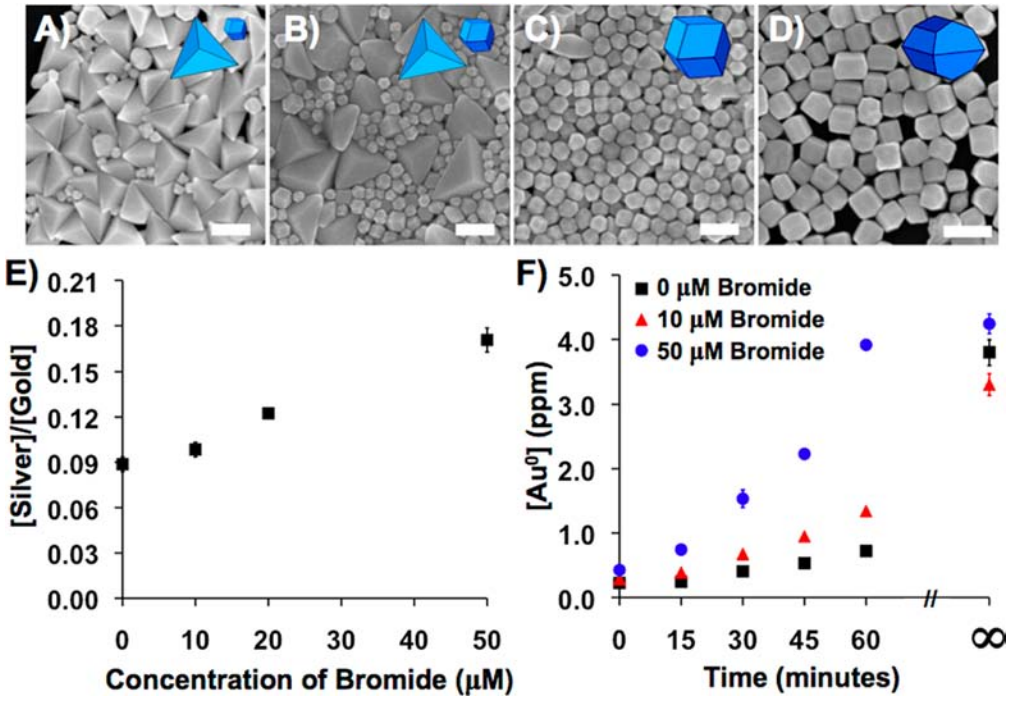

Figure 6. (A–D) SEM images of reaction products from growth solutions containing 40 mM CTA-Cl, 10 μM $AgNO_3$, and (A) 0.0, (B) 10, (C) 20, and (D) 50 μM NaBr. Scale bars: 200 nm. In the absence of bromide, a mixture of {110}-faceted bipyramids and {110}-faceted rhombic dodecahedra are produced. With increasing bromide, the size and yield of the bipyramids decrease while the size and yield of the rhombic dodecahedra increase. At 50 μM bromide, {310}-faceted truncated ditetragonal prisms are generated. (E) XPS data on the silver/gold ratio for particles generated with different concentrations of bromide in the growth solution, showing that as the bromide concentration is increased the silver content on the surface of each particle also increases. (F) ICP-AES kinetics data of the reactions containing 0 μM (black squares), 10 μM (red triangles), and 50 μM (blue circles) NaBr.

due to the decreasing favorability of the Ag–halide interaction and an increasing favorability of the Au–halide interaction in that same ordering.[69] In other words, there is a strong driving force for the formation of an $Au–Ag_{UPD}–Cl$ surface structure and this driving force is much less for the formation of an $Au–Ag_{UPD}–Br$ surface and even less still for an $Au–Ag_{UPD}–I$ structure.

In the following experiments, we demonstrate how the previously described influence of halides on the underpotential deposition of silver can be used to direct particle growth under conditions where the halide concentration in the reaction is less than the concentration of gold ion. Growth solutions were prepared having the appropriate concentrations of reagents to produce rhombic dodecahedra, notably a 10 μM concentration of Ag^+ in 40 mM CTA-Cl, 60 mM NaCl, 18 mM HCl, 0.5 mM $HAuCl_4$, 1.0 mM ascorbic acid, and 0.1 μL of 7 nm diameter seeds, with the modification that each solution also contained a small amount of NaBr (0, 10, 20, or 50 μM; Chart S1). SEM images of the products indicate that, with increasing amounts of bromide, the yield of the {110}-faceted rhombic dodecahedra increases compared to the yield of the {110}-faceted bipyramids until rhombic dodecahedra become the primary product at 20 μM bromide and eventually truncated ditetragonal prisms are dominant at 50 μM bromide (Figure 6A–D). This is an intriguing result, since more silver is required to stabilize the {310} facets of the truncated ditetragonal prisms than for the {110} facets of the rhombic dodecahedra, yet in this case both growth solutions contain the same amount of silver ions. In other words, by keeping the Ag^+ concentration in the growth solution constant, the amount of silver on the particle surface can be increased by introducing bromide. XPS was used to quantify the silver/gold ratio on the surface of these particles (Figure 6E and Figure S2 (Supporting Information)). As would be expected on the basis of the particle shapes observed, the amount of silver on the surface of each particle increases as the facets become more open (i.e., higher index), and this is correlated with increasing concentrations of bromide in the growth solution. The ratios of silver to gold on the surface of the particles are also consistent with what would be expected for these shapes on the basis of the results of our previous study of silver ion as an additive (Figure S3, Supporting Information).[26]

ICP-AES monitoring of the rate of particle formation for these reactions suggests that, in the presence of silver ions, increasing amounts of bromide result in an acceleration of the rate of particle formation (Figure 6F). This observation is in stark contrast to the previously discussed experiments where, in the absence of silver, the addition of bromide resulted in a decreased rate of particle formation. To confirm the validity of these results, a second set of reactions was studied which involved growth solutions containing not only the appropriate concentrations of reagents for generating {310}-faceted truncated ditetragonal prisms (including 40 μM Ag^+) but also a 40 μM concentration of bromide (Chart S1). Consistent with the above results, the addition of bromide to these reactions resulted in the formation of concave cubes, rather than the truncated ditetragonal prisms that would have been observed in the absence of added bromide (Figure S4, Supporting Information). As before, by adding bromide, we can induce the formation of a particle shape with higher-index facets than that which would form at the same silver ion concentration in the absence of bromide. XPS was used to confirm that, as would be

dx.doi.org/10.1021/ja305245g | J. Am. Chem. Soc. 2012, 134, 14542–14554

expected from the particle shapes, the concave cubes formed in this reaction have a higher concentration of silver on their surface than the truncated ditetragonal prisms (Figures S3 and S4).

Shape control similar to that achieved with bromide is observed when small amounts of iodide are introduced to the reaction in the presence of silver. This is illustrated by a set of reactions containing 10 μM silver and 0.00, 0.01, 0.05, or 0.10 μM iodide. In the absence of iodide, {110}-faceted rhombic dodecahedra and bipyramids are formed. When more iodide is present in the growth solution, the rhombic dodecahedra become larger in size and are the dominant product over bipyramids until truncated ditetragonal prisms form at 0.10 μM iodide (Figure S5, Supporting Information). XPS data confirm that, as more iodide is added to the growth solution, more silver is deposited onto the surface of each particle (Figure S5). Furthermore, ICP-AES shows that, with increasing amounts of iodide, the initial rate of particle formation increases (Figure S5). Taken together, these results concerning the behavior of iodide in the presence of silver ions are analogous to those observed for the behavior of bromide in the presence of silver ions, yet the iodide concentration necessary to observe these differences in the shape of the nanoparticles is 2 orders of magnitude lower than what is necessary for bromide, consistent with observations in the absence of silver ions.

The overall trend observed in these experiments is that, when trace amounts of bromide or iodide are added to growth solutions containing a silver ion additive in CTA-Cl, more silver is deposited onto the surface of the gold nanoparticles than is deposited in the absence of the bromide or iodide ions. Concurrently, when more silver is deposited onto the particle surface, a more open and higher-index surface is stabilized, consistent with an underpotential deposition-controlled growth mechanism.[26] Moreover, the addition of either bromide or iodide to these reactions leads to an increased rate of particle growth. Initially, these observations may seem counterintuitive, since bromide and iodide bind more strongly to the gold particle surface than does chloride and thus could inhibit the deposition of silver onto the particle surface. However, these results are consistent with the influence of halides on the stability of Ag_{UPD} layers on a gold surface. The addition of either bromide or iodide to these reactions induces a destabilization of the Ag_{UPD} layer, with the destabilizing effect being more significant for iodide than for bromide. We hypothesize that when bromide or iodide destabilizes the Ag_{UPD} layer, more opportunities are created for silver to rearrange on the particle surface, either through a cycle of oxidation and redeposition or through local surface mobility.[68−72] This mobility facilitates the relocation of silver to more energetically favorable surface sites, such as corners or atomic steps, thus allowing facets with more exposed surface atoms to be stabilized at lower concentrations of silver ions than would be required in the presence of chloride only. The higher mobility imparted to the Ag_{UPD} layer by bromide or iodide as compared to chloride also results in a faster rate of gold ion reduction onto the particles because the more dynamic surface is more easily accessible for gold deposition. This behavior explains both the XPS and ICP-AES data, which show that increasing concentrations of either bromide or iodide in the growth solution lead to both greater amounts of silver on the surface of each particle and faster rates of gold ion reduction. This relatively high stability of an Ag_{UPD} layer in the presence of chloride also explains why the use of silver underpotential deposition is a very effective means for controlling particle shape in reactions conducted in CTA-Cl, since the overall strength of the Au−Ag_{UPD}−Cl interaction makes the reactions very sensitive to the concentration of silver ions in the growth solution, thereby enabling the synthesis of a wide variety of particle shapes. Therefore, if one wants to work under kinetically controlled growth conditions, it is more optimal to work in a chloride-containing surfactant than one comprised of bromide or iodide.

Effects of High Concentrations of Halides in the Presence of Silver Ions. Thus far, the effects of adding small amounts of bromide or iodide to growth solutions containing a chloride-containing surfactant and silver ions have been explored. In this section, we demonstrate that high concentrations of either bromide or iodide in the presence of silver ions will actually inhibit the underpotential deposition of silver onto the gold particle surface because of the strong binding of these halides to gold surfaces. However, due to the destabilizing effects that these halides have on the Ag_{UPD} layer, high-index facets can still be stabilized despite the lower coverage of silver. These results are relevant when, for example, a bromide-containing surfactant is used rather than a chloride-containing surfactant, and this distinction is the difference between producing concave cubes[24] and tetrahexahedra,[22] which are prepared from growth solutions containing 100 μM silver and either 100 mM CTA-Cl or CTA-Br, respectively (in addition to 0.5 mM $HAuCl_4$, 1.0 mM ascorbic acid, 20 mM HCl, and 0.1 μL of 7 nm diameter seeds; Chart S1).

First, a combination of XPS and ICP-AES was used to characterize and compare the metallic compositions of the tetrahexahedra and concave cubes. Following the same protocol as described previously, XPS characterization of the surface silver/gold ratio of the tetrahexahedra reveals that the tetrahexahedra have a significantly lower silver coverage ($Ag/Au_{tetrahexahedra}$ = 0.14) than the concave cubes ($Ag/Au_{concave\ cubes}$ = 0.26) (Figure 7). The XPS results were confirmed by ICP-AES, a complementary technique. Because the ICP-AES analysis is a bulk characterization technique, the silver coverage can be expressed in terms of a percentage of a monolayer.[26] In comparison

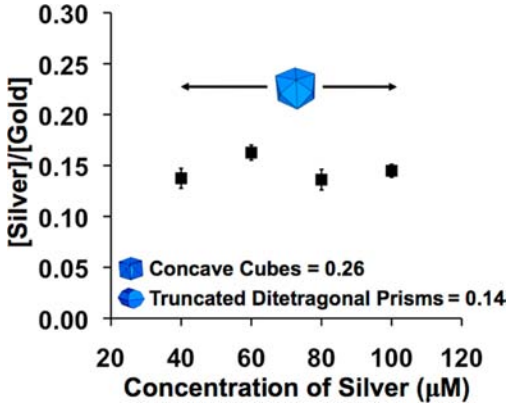

Figure 7. XPS data on the silver/gold ratio for particles generated in 100 mM CTA-Br with different concentrations of $AgNO_3$ in the growth solution. In the range of 40−100 μM silver ions, all of the products formed in CTA-Br are tetrahexahedra and have similar silver/gold ratios. In the case of CTA-Cl, 40 μM silver ions yields truncated ditetragonal prisms that have a silver/gold ratio of 0.14, while 100 μM silver ions yield concave cubes that have a silver/gold ratio of 0.26, as shown in the figure. Even though the surface facets of the tetrahexahedra and concave cubes are similar, the tetrahexahedra have a surface silver/gold ratio closer to that of the truncated ditetragonal prisms than to that of the concave cubes.

to the 84% of a monolayer silver coverage on the concave cubes, the silver coverage on the tetrahexahedra is only 47% of a monolayer, as determined by ICP-AES (Figure 8). Both characterization techniques corroborate a lower coverage of silver on the tetrahexahedra than the concave cubes, reflecting a difference in the behavior of silver ions in the presence of either bromide or chloride.

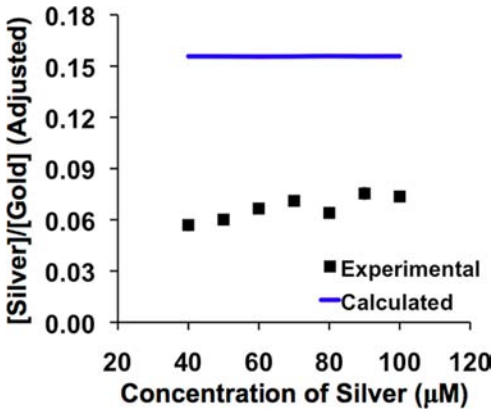

Figure 8. ICP-AES data plotting the experimentally determined bulk silver/gold ratio (black squares) of tetrahexahedra prepared from growth solutions with silver ion concentrations ranging from 40 to 100 μM. Also plotted is a calculated value for the silver/gold ratio expected for a monolayer coverage of silver for a {730} facet (blue line). These data reveal that the tetrahexahedra have approximately a 47% monolayer coverage of silver that decreases to 37% with decreasing concentrations of silver in the growth solution. Note that these silver/gold ratios determined by ICP-AES are normalized for both the size and shape of the nanoparticles and thus represent a value reflecting the silver coverage on the particle surface. See ref 26 for a more detailed discussion of this adjustment.

To further probe the behavior of silver ions in CTA-Br, the concentration of silver in the tetrahexahedra growth solution was varied from 40 to 100 μM. This is an important range of silver ion concentration for reactions conducted in CTA-Cl, where at 40 μM Ag^+, {310}-faceted truncated ditetragonal prisms are formed, while at 100 μM Ag^+, {720}-faceted concave cubes are formed. In addition to the dramatic difference in particle morphology observed at these two different concentrations of silver in CTA-Cl, there is also a distinct change in surface silver coverage due to the different number of exposed surface atoms associated with the crystallographic facets which enclose each particle shape.[26] However, when CTA-Br is used rather than CTA-Cl in the growth solution, a different behavior is observed. SEM characterization of the products formed from growth solutions containing 100 mM CTA-Br and silver ion concentrations ranging from 40 to 100 μM reveals that tetrahexahedra are produced at all concentrations of silver ions tested (Figure S6, Supporting Information). There is also little to no change in the dimensions of the tetrahexahedra at different concentrations of silver ions. Characterization of the silver content by XPS (Figure 7) and ICP-AES (Figure 8) shows a relatively constant silver coverage, regardless of the silver ion concentration in the growth solution. While there is a decrease in the amount of silver on the surface of the tetrahexahedra from the 47% monolayer coverage at 100 μM silver in the growth solution to a 37% monolayer coverage of silver at 40 μM silver in the growth solution, this decrease does not affect the shape of the particles.

These results, obtained from growth solutions containing a high concentration (100 mM) of CTA-Br, are markedly different from the case where a small concentration of bromide (<50 μM) and a high concentration (100 mM) of CTA-Cl are both present in the growth solution. While the addition of small amounts of bromide to CTA-Cl results in an increase in the amount of silver deposited onto the gold nanoparticles, a high concentration of bromide in the form of CTA-Br inhibits the deposition of silver in comparison to the use of CTA-Cl. This behavior can be attributed to the same behavior of bromide that was previously discussed, namely (1) the decreased stability of the Ag_{UPD} layer in bromide as compared to chloride[54,68−72] and (2) bromide binding more strongly to the gold particle surface than chloride.[54] The ability of bromide to destabilize and create a more dynamic Ag_{UPD} layer facilitates the rearrangement of silver to more thermodynamically favorable surface sites, such as atomic steps, and enables the stabilization the {730} facets of the tetrahexahedra even though the surface coverage of silver is significantly lower than the {720}-faceted concave cubes. Additionally, a second contributing factor to the lower silver coverage on the tetrahexahedra is the higher binding affinity of bromide for the gold surface in comparison to that of chloride, which enables bromide to inhibit the deposition of silver by blocking the gold surface.

We have experimentally demonstrated the enhanced binding of bromide compared to chloride to the gold particle surface and the destabilization of the Ag_{UPD} layer by bromide in the following experiments. First, growth solutions were prepared containing either 100 mM CTA-Cl and 100 mM NaBr or 100 mM CTA-Br and 100 mM NaCl in addition to 0.5 mM $HAuCl_4$, 1.0 mM ascorbic acid, 20 mM HCl, and 0.1 μL of 7 nm diameter seeds (Chart S1). The products of both reactions were tetrahexahedra (Figure S7, Supporting Information). In other words, if bromide is present in the reaction at high concentrations (100 mM), in the form of either a salt (NaBr) or a surfactant (CTA-Br), then the effects of bromide dominate the effects of chloride (even if the chloride concentration is also high, 100 mM) and tetrahexahedra are produced. Next, we demonstrate that more silver can be deposited onto the gold particle surface by reducing the bromide concentration in the growth solution. In one experiment, a growth solution was prepared with 10 μM silver ion ($^1/_{10}$th of the silver concentration typically used in the tetrahexahedra synthesis) and 100 mM CTA-Br (plus 0.5 mM $HAuCl_4$, 1.0 mM ascorbic acid, 20 mM HCl, and 0.1 μL of 7 nm diameter seeds). The products of this reaction display facets but are very polydisperse, indicative of uncontrolled growth (Figure S8, Supporting Information). Note that this is in contrast to the analogous experiment in CTA-Cl, where rhombic dodecahedra are produced. Importantly, we found that by decreasing the CTA-Br concentration by a factor of 4, we were able to observe the growth of tetrahexahedra (Figure S8). This indicates that, when the concentration of bromide was reduced, more silver was deposited onto the gold particles, allowing the stabilization of the high-index facets of the tetrahexahedra. In another experiment, a very high concentration of silver ions (>100 μM) was used in the growth solution of a reaction seeded with concave cubes (Chart S1). When CTA-Cl is used as a surfactant, since the concentration of silver ions is extremely high (500 μM), {111} facets can be stabilized, because those facets have the highest number of exposed surface atoms (i.e., they are the most densely packed).[35] The analogous experiment can be conducted in CTA-Br; however, the product observed is simply overgrown concave cubes (Figure S9,

dx.doi.org/10.1021/ja305245g | J. Am. Chem. Soc. 2012, 134, 14542−14554

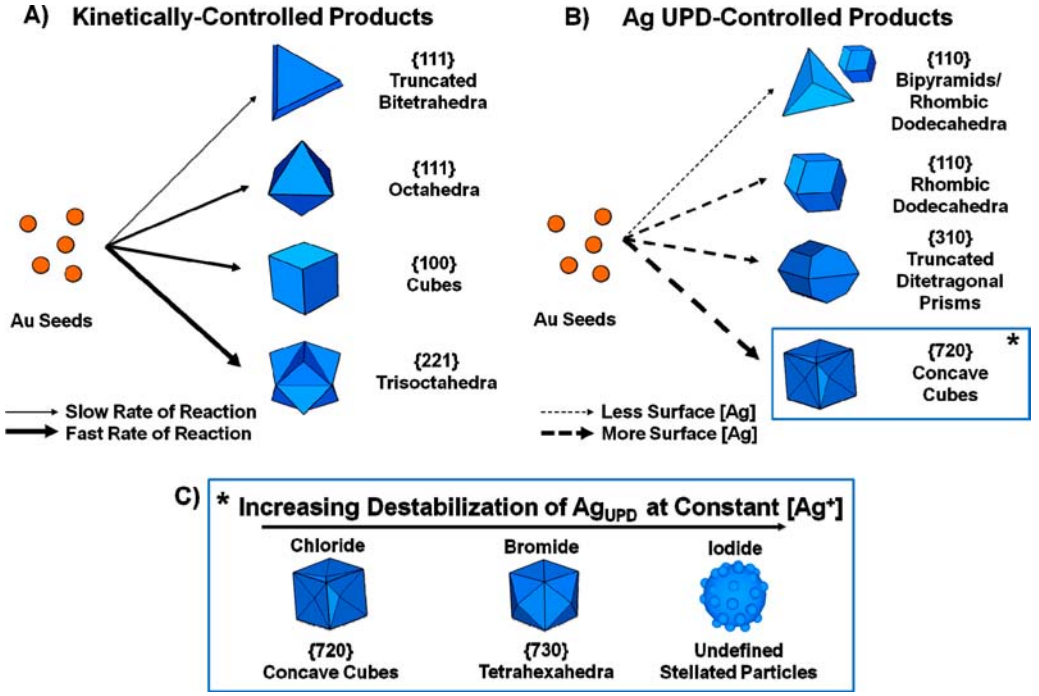

Figure 9. Scheme illustrating how halides and silver ions can be used to direct the growth of gold seeds down different growth pathways to yield different shaped products: (A) kinetically controlled products in the absence of silver ions; (B) Ag underpotential deposition-controlled products where the interactions of silver with the particle surface dictate product shape; (C) effect of varying the stability of the Ag_{UPD} layer with high concentrations of chloride, bromide, or iodide in the growth solution, yielding concave cubes, tetrahexahedra, and stellated particles, respectively.

Supporting Information). This indicates that, even at high silver ion concentrations, the bromide is inhibiting the deposition of silver onto the particle surface and thus preventing the formation of {111}-faceted octahedra. However, when the CTA-Br concentration is reduced to 20 mM, thereby reducing the total bromide concentration in the growth solution, the formation of {111}-faceted octahedra is observed (Figure S9). In the same manner as the first experiment, reducing the bromide concentration enables more silver to be deposited onto the gold surface of each particle.[19] Taken together, this set of experiments further confirms our hypothesis that, at high concentrations of bromide in the growth solution, the deposition of silver onto the surface of the gold particles is inhibited.

While we expect to observe the same trend in behavior with iodide, the insolubility of CTA-I prevents the study of iodide at high concentrations. However, iodide can be added to solution up to a concentration that is equal to that of the gold ion in the growth solution, and experiments conducted in this range of iodide concentrations are in agreement with expected behavior. When the growth solution contains 10 μM iodide and 100 mM CTA-Cl, particles with extremely stellated features are produced (Figure S10, Supporting Information). This particle morphology most likely arises from poorly controlled growth as a result of iodide both binding to the particle surface and severely destabilizing the Ag_{UPD} layer. It is possible that silver deposited onto the gold particle surface is rapidly displaced or destabilized by iodide, and this poorly controlled growth results in the generation of particles with stellated features and ill-defined surface facets.

Concave versus Convex High-Index Faceted Nanoparticles. It is now understood why the combination of silver ions with chloride- or bromide-containing surfactants yields related high-index faceted nanostructures: concave cubes and tetrahexahedra, respectively. However, one important point not yet addressed is why the concave cubes have concave features while the tetrahexahedra are convex nanostructures. Regardless of the synthetic method used, concave nanostructures are unusual, but their growth is typically favored under kinetically controlled growth conditions.[25,49,73−78] We hypothesize that the convex tetrahexahedra are overall more thermodynamically favorable structures than the concave cubes due to their more isotropic shape. We believe that the concavity of the concave cubes is due to the relatively high stability of the Ag_{UPD} layer in the presence of chloride and the rapid rate of gold ion reduction in CTA-Cl, which enables the formation of less thermodynamically favorable shapes. Effectively, the underpotential deposition of silver in the presence of a chloride-containing surfactant "locks in" a certain surface facet early in the reaction because of the stable Ag_{UPD} layer formed in chloride. For example, even at the early stages of the concave cube reaction, transmission electron microscopy (TEM) images show that the small growing seed particles are in the shape of small concave cubes (Figure S11, Supporting Information). Over the course of the reaction, the small concave cubes continue to grow, maintaining their shape, until they reach their final size. We have found that smaller diameter (~7 nm) seed particles are crucial for the growth of concave cubes, presumably due to the higher reactivity of smaller seeds. This is demonstrated when seeds with a diameter of ~40 nm are used and, rather than concave cubes, truncated ditetragonal prisms are formed even at concentrations of silver ions that would normally produce concave cubes (100 μM silver ion). It is possible that the large seeds are not reactive enough to support the growth of concave features. The energy barrier for growing concave features may be too high for these larger seeds to overcome. It then follows that, when a bromide-containing surfactant is used, the slower reduction rate of $[AuBr_2]^-$ in comparison to that of $[AuCl_2]^-$ and the decreased stability of the Ag_{UPD} layer in bromide results

dx.doi.org/10.1021/ja305245g | J. Am. Chem. Soc. 2012, 134, 14542−14554

in the development of convex, rather than concave, features due to rearrangement of the surface atoms into a more thermodynamically favorable convex structure.

DISCUSSION

Design Considerations for Controlling Particle Growth. Considering the results from all of the previously discussed experiments, we now can explain the roles of silver ions and halides in seed-mediated syntheses and how they can be used to control particle shape and surface facet structure (Figure 9). Essentially, in the absence of silver ions, the rate of reaction is the dominant factor that controls product growth. Slower rates of reaction yield lower-energy surface facets and can be achieved by using a lower amount of ascorbic acid or by introducing a larger halide (bromide or iodide). In the presence of silver ions as an underpotential deposition agent, surface effects are more influential than kinetic effects in controlling particle growth, with higher amounts of silver on the particle surface yielding higher-index surfaces. More silver can be deposited onto the particle surface by increasing the amount of silver ion in the growth solution or by introducing a trace amount of bromide or iodide. However, at high concentrations of halides, the Ag_{UPD} layer is destabilized and the binding of the halide to the particle surface inhibits the deposition of silver, although the very dynamic particle surface due to the destabilized Ag_{UPD} layer can still yield high-index faceted tetrahexahedra with a bromide-containing surfactant. However, these effects are not suitable for achieving well-faceted particles in the presence of iodide. In contrast, the very stable Ag_{UPD} layer in the presence of chloride can "lock-in" the concave features of the concave cubes early in growth while the seeds are small and highly reactive. Although it would be ideal to measure the amount of halides on the surface of the nanoparticles to further confirm our results, this is not possible to do by XPS due to some of the silver halide peaks overlapping with peaks for silver without a bound halide.

Here we provide six design considerations that expand upon the above discussion. These design considerations can be followed to rationally control product shape in the seed-mediated synthesis of gold nanoparticles.

(1) *Increasing the concentration of ascorbic acid speeds the rate of gold ion reduction, and thus particle growth, leading to more kinetically favored particles with higher-energy surface facets.* This is based on the observation that {111}-faceted octahedra, {100}-faceted cubes, and {221}-faceted trisoctahedra form at 0.5, 2.0, and 10.0 mM ascorbic acid, respectively.

(2) *In the absence of other shape-directing additives, and under otherwise identical conditions, the addition of a larger halide will slow particle growth, facilitating the synthesis of particles with lower-energy surface facets.* This is based on the observation of a trend in particle shapes opposite to that observed with increased ascorbic acid and is supported by ICP-AES kinetics data. The slowed growth is due to a decrease in the reduction potential and solubility of the Au^+-halide complexes formed in solution in the order $[AuCl_2]^- > [AuBr_2]^- > [AuI_2]^-$, as well as an increasing binding affinity of the larger halides for the gold surface in the order $Cl^- < Br^- < I^-$. Thus, more thermodynamically favorable products form with increasing concentrations of bromide and iodide, with the effects of iodide being stronger than those of bromide.

(3) *In the absence of larger halides (bromide and iodide), increasing concentrations of silver ions stabilize particles with a greater number of exposed surface atoms per unit surface area, enabling the formation of high-index nanostructures.* This design consideration is consistent with the observed formation of octahedra, rhombic dodecahedra, truncated ditetragonal prisms, and concave cubes at increasingly larger concentrations of silver ion in solution and is confirmed by XPS and ICP-AES surface characterization as well as kinetics studies.[26] The underpotential deposition of up to a monolayer of silver onto a particular surface facet on a growing gold particle inhibits further gold deposition on that surface, and the facet is maintained in the final particle shape. A given concentration of silver ions will stabilize the most densely packed facet for which there is sufficient silver to deposit a near-monolayer onto.

(4) *In the presence of silver ion as a shape-directing additive, the addition of a trace amount of a larger halide decreases the stability of the Ag_{UPD} layer, and particles with more open facets can be synthesized without adding as much silver ion.* We have observed that, in the presence of trace bromide or iodide, particles with more open facets, such as truncated ditetragonal prisms, are stabilized at a concentration of silver ion in solution that, in the presence of chloride only, would lead to the growth of a particle bound by lower-energy facets, such as rhombic dodecahedra. This observation is further supported by XPS surface characterization and ICP-AES kinetics experiments. Chloride acts to stabilize the Ag_{UPD} layer, while bromide and iodide destabilize the Ag_{UPD} layer, with iodide having greater destabilizing effects than bromide. This is due to the increasing strength of the gold–halide interaction relative to the silver–gold and silver–halide interactions. At low halide concentrations, when the halide is bromide or iodide, the decreasing stability of the Ag_{UPD} layer results in greater silver coverage via underpotential deposition and thus more open (higher-index) surfaces form at lower silver ion concentrations.

(5) *In the presence of silver ions as a shape-directing additive, the addition of a large amount of a larger halide (bromide and iodide) greatly decreases the stability of the Ag_{UPD} layer and blocks silver deposition, limiting the number of particle shapes that can form.* This conclusion is based on experiments which show that at high halide concentrations, where the halide is bromide or iodide, this destabilizing effect results in a lower surface silver coverage, due to the strong binding affinity of bromide and iodide for the gold surface, blocking silver deposition. Consequently, for bromide, high-index {730} surfaces can still be formed due to the mobility of the Ag_{UPD} layer, but for iodide, this enhanced mobility results in surfaces that are not well-defined.

(6) *The enhanced stability of the Ag_{UPD} layer in the presence of chloride causes growing gold nanoparticles to become kinetically "trapped" or "locked" into a particular facet structure early in their growth, enabling the formation of a wide variety of shapes as well as concave particles.* This is supported by the observation that the shape of the concave cubes is fixed very early in their growth. As a result of this kinetic trapping, a greater variety of shapes can form in the case of chloride than in the case of bromide, where the Ag_{UPD} layer is more mobile and can reach more of an energy minimum.

dx.doi.org/10.1021/ja305245g | J. Am. Chem. Soc. 2012, 134, 14542–14554

These design considerations are self-consistent and accurately describe all of the experimental observations discussed in this article. In addition to explaining the formation of the 10 classes of nanoparticles of different shape, including concave cubes and tetrahexahedra, this study also has implications in explaining previous results beyond high-index nanostructures. In our previously published syntheses for gold nanoprisms, we have reported that trace amounts of iodide are vital for the formation of nanoprisms.[21] Our results here suggest that this is likely due to the decrease in reaction rate caused by iodide in the absence of silver as a result of a lowered reduction potential and solubility for $[AuI_2]^-$ as well as surface binding effects of iodide. In addition, our study lends some insight to the mechanism of formation of gold nanorods in reaction solutions containing silver ion in CTA-Br.[16] In this case, it is observed that the rods increase in length with the addition of larger amounts of silver ion. Others have suggested that these rods are in fact high-index faceted structures, analogous to tetrahexahedra with high aspect ratios.[79,80] We have shown that the variety of high-index gold nanostructures stabilized by silver in CTA-Br is limited, and thus, in the case of rods, rather than stabilizing a more open surface facet, the Ag_{UPD} layer, which is highly mobile in 100 mM CTA-Br, expands to cover a larger area with the same facet structure. The observed result of this process is that an increase in silver ion concentration leads to an increase in rod aspect ratio, as high aspect ratio structures have a larger surface area relative to their volume. Further, such conclusions are in agreement with work reported by Guyot-Sionnest and co-workers regarding the control of gold nanorod growth via silver underpotential deposition as well as their synthesis of penta-twinned bipyramids.[23] The silver serves to passivate the surface in both cases, and it is shown that the controlling factor in the growth of the bipyramids is the use of penta-twinned seeds, which forces the growth of the penta-twinned bipyramids rather than single crystalline rods. Despite differences in crystallinity, these two structures both have high-index facets, likely with comparable surface silver coverages as a result of the destabilizing effects of bromide of Ag_{UPD}.[23,79,80]

We have shown in this article that the two major factors controlling particle growth are reaction kinetics and surface passivation effects (particularly by silver), and these general design considerations likely can also be applied to syntheses other than those which use a CTA-X surfactant. For example, Xu and co-workers have reported the synthesis of rhombic dodecahedra, octahedra, and cubes from single-crystalline seeds in cetylpyridinium chloride (CPC).[36] The reaction product is changed from {110}-faceted rhombic dodecahedra to {111}-faceted octahedra by significantly decreasing the ascorbic acid concentration, leading to a lower-energy facet at a slower reaction rate, as predicted by our design considerations. Cubes bound by {100} facets are generated by adding a large amount of bromide to the slower set of reaction conditions. This initially seems contradictory to our work, since in our studies the addition of such a large concentration of bromide to the reaction would lead to the formation of bitetrahedra, which favor growth along a twin plane due to slow, kinetically controlled growth conditions. However, it is important to note that the seeds used to initiate nanoparticle growth in the work by Xu and co-workers are single crystalline and also somewhat cubic or rodlike in shape.[36] Since the single-crystalline seeds do not contain twin planes where lateral growth can take place, it is possible that a slow layer-by-layer overgrowth of the seeds occurs instead and the final cube structure reflects the original shape of the seed particles. Recently, there has been great interest in gold nanostars, synthesized in CTAB,[15,81] or in a system containing gold, poly(vinylpyrrolidone) (PVP), and *N*,*N*-dimethylformamide (DMF).[82] In both cases, it has been proposed that the growth of these stars occurs due to rapid kinetic growth.[15,81,82] Such extremely rapid growth fits into our scheme at reaction rates faster than those which produce trisoctahedra, where growth becomes less controlled and leads to polycrystalline and stellated structures. A similar situation is also observed in the case of our reactions involving both silver ion and iodide. While some of the principles we have outlined here, such as kinetic control, may also be applicable to the polyol process, the reaction conditions employed in that method are vastly different from those of the seed-mediated synthesis and therefore it is beyond the scope of this work to speculate on such connections. However, we note that while the polyol process is the preferred method for the synthesis of shape-controlled nanoparticles composed of silver and other metals, the seed-mediated synthesis is one of the most popular, if not the most popular, methods used by the nanoscience community to generate gold nanoparticles.[9] Thus, the design considerations outlined here should be of great utility in advancing the shape-controlled synthesis of gold nanoparticles.

■ CONCLUSIONS

Collectively, these data provide an understanding of the role of silver ions and halides in seed-mediated syntheses of gold nanoparticles, and they show how two different sets of particle shapes (Figure 9A,B) can be accessed via kinetic control, surface passivation, or a combination of both, in either the absence or presence of silver ions. The mechanistic insight and design considerations put forth in this study have been used to explain a number of previously reported nanoparticle syntheses, such as those involving the formation of concave cubes, tetrahexahedra, trisoctahedra, rods, and prisms. These design considerations will also serve as guiding principles for further work in this area, including studies directed at understanding how twinned structures[5,9] fit within the framework of kinetic- and surface-controlled nanoparticle growth. In addition, similar interactions may be integral in the synthesis of nanoparticles of other metals, where metal−halide interactions and underpotentially deposited metals are involved in controlling particle shape. For example, work by Xia and co-workers has shown that reaction kinetics are key in directing the growth of nanoparticles composed of other metals, such as silver, platinum, palladium, and rhodium.[9,61,83] Ultimately, the design considerations presented as a culmination of this study represent a step toward the rational synthesis of gold nanoparticles of desired shapes, an advance required for the use of these nanoparticles in many applications.

■ EXPERIMENTAL SECTION

Chemicals and Materials. Gold(III) chloride trihydrate ($HAuCl_4 \cdot 3H_2O$, 99.9+%), silver nitrate ($AgNO_3$, 99.9999%), sodium borohydrate ($NaBH_4$, 99.99%), sodium chloride (NaCl, 99.999%), sodium bromide (NaBr, 99.0+%), sodium iodide (NaI, 99.999%), L-ascorbic acid (AA, 99+%), cetyltrimethylammonium chloride (CTA-Cl, 25 wt % in H_2O), and cetyltrimethylammonium bromide (CTA-Br, 99%) were purchased from Aldrich and used without further purification. Hydrochloric acid (HCl, 1 mol/L volumetric solution) was purchased from Fluka and used without further purification.

Preparation of Seed Particles. Au seeds with a diameter of 7 nm were prepared by quickly injecting 0.60 mL of ice-cold, freshly prepared $NaBH_4$ (10 mM) into a rapidly stirred solution containing 0.25 mL of $HAuCl_4$ (10 mM) and 10.00 mL of CTA-Cl (100 mM) or

CTA-Br (100 mM). The seed solution was stirred for 1 min and then left undisturbed for 2 h. Larger seeds were prepared by growing the 7 nm diameter seeds into 40 nm diameter Au seeds by consecutively adding 200.0 μL $HAuCl_4$ (10 mM) and 40.0 μL AA (100 mM) to a solution containing 8.0 mL of H_2O and 1.6 mL of 100 mM CTA-Cl. The 7 nm diameter seed particles were diluted in 100 mM CTA-Cl (or CTA-Br) to generate a solution which was $^1/_{10}$ the concentration of the original seed solution. Growth of 40 nm diameter seed particles was initiated by adding 100.0 μL of the diluted 7 nm diameter seeds. The reaction mixture was swirled immediately after the addition of the seeds and then left undisturbed on the benchtop until the reaction was complete.

Typical Seed-Mediated Synthesis. A typical growth solution was prepared by consecutively adding reagents into 10.00 mL of CTA-Cl (or CTA-Br) in the following order, as necessary (Chart S1): NaCl, HCl to adjust pH, 0.50 mL of $HAuCl_4$ (10 mM), NaBr or NaI, $AgNO_3$ (10 mM), and then 0.10 mL of AA (100 mM). The 7 nm diameter seeds were serially diluted in 0.1 M CTA-Cl to generate a solution which was $^1/_{1000}$ the concentration of the original seed solution. Particle growth was initiated by adding 100.0 μL of the diluted 7 nm diameter seeds or 0.5 mL of the 40 nm diameter seeds to the growth solution, as required (Chart S1). The reaction mixture was swirled immediately after the addition of the seeds and then left undisturbed on the benchtop until the reaction was complete.

Instrumentation. Scanning electron microscopy (SEM) images were obtained using a Hitachi S-4800-II cFEG SEM. Transmission electron microscopy (TEM) images were obtained using a Hitachi HD-2300 STEM. Inductively coupled plasma-atomic emission spectrometry (ICP-AES) analysis was performed using a Varian Vista ICP-AES. Samples were prepared for ICP-AES by removing aliquots of the reactions at various time points, quenching the reactions with an amount of BSPP in excess of the gold concentration in the reaction, and then centrifuging the particles twice to isolate the particles from the reaction solution. The particles were then dissolved in fresh aqua regia and subsequently diluted with NANOpure H_2O just prior to ICP-AES analysis. X-ray photoelectron spectroscopy (XPS) was conducted using an Omicron ESCA Probe XPS spectrometer. Samples were prepared for XPS by centrifuging particle solutions to concentrate them, resuspending the particles in NANOpure H_2O, and repeatedly dropcasting the particles onto a silicon substrate. XPS spectra were gathered using an Al Kα (1486.5 eV) anode with a power of 200 W (20 kV) and a hemispherical energy analyzer operated at a pass energy of 70.0 eV for survey scans and 24 eV for high-resolution scans.

■ ASSOCIATED CONTENT

Supporting Information

A chart and figures, including a chart of reaction conditions, additional SEM images, representative XPS spectra, XPS data comparing surface composition at various silver and bromide concentrations, XPS data for growth solutions containing 40 μM silver ion and bromide, ICP-AES kinetics and XPS data for growth solutions containing silver and iodide, and TEM images of concave cubes at early stages of growth. This material is available free of charge via the Internet at http://pubs.acs.org.

■ AUTHOR INFORMATION

Corresponding Author

*E-mail: chadnano@northwestern.edu

Present Address

‡Department of Chemistry, University of Nebraska, Lincoln, NE 68588.

Author Contributions

†These author contributed equally.

Notes

The authors declare no competing financial interest.

■ ACKNOWLEDGMENTS

This work was supported by AFOSR Awards FA9550-11-1-0275 and FA9550-09-1-0294, DoD/NSSEFF/NPS Award N00244-09-1-0012, Non-equilibrium Energy Research Center (NERC) DOE Award DE-SC0000989, Nanoscale Science and Engineering Initiative NSF Award EEC-0647560, NSF MRSEC (DMR-0520513 and DMR-1121262), and shared facilities at the Materials Research Center. Microscopy work was performed in the EPIC facility of the NUANCE Center, which is supported by the NSF-NSEC, NSF-MRSEC, Keck Foundation, the state of Illinois, and Northwestern University (NU). XPS experiments were performed at the Keck-II facilities at NU. M.L.P. gratefully acknowledges support from the DoD through the National Defense Science & Engineering Graduate (NDSEG) Fellowship Program (32 CFR 168a).

■ REFERENCES

(1) Hurst, S. J.; Payne, E. K.; Qin, L.; Mirkin, C. A. *Angew. Chem., Int. Ed.* **2006**, *45*, 2672.
(2) Jin, R.; Cao, Y.; Mirkin, C. A.; Kelly, K. L.; Schatz, G. C.; Zheng, J. G. *Science* **2001**, *294*, 1901.
(3) Millstone, J. E.; Park, S.; Shuford, K. L.; Qin, L.; Schatz, G. C.; Mirkin, C. A. *J. Am. Chem. Soc.* **2005**, *127*, 5312.
(4) Millstone, J. E.; Hurst, S. J.; Métraux, G. S.; Cutler, J. I.; Mirkin, C. A. *Small* **2009**, *5*, 646.
(5) Tao, A. R.; Habas, S.; Yang, P. *Small* **2008**, *4*, 310.
(6) Jin, R.; Cao, Y. C.; Hao, E.; Métraux, G. S.; Schatz, G. C.; Mirkin, C. A. *Nature* **2003**, *425*, 487.
(7) Yoo, H.; Millstone, J. E.; Li, S.; Jang, J.-W.; Wei, W.; Wu, J.; Schatz, G. C.; Mirkin, C. A. *Nano Lett.* **2009**, *9*, 3038.
(8) Zhang, J.; Li, S.; Wu, J.; Schatz, G. C.; Mirkin, C. A. *Angew. Chem., Int. Ed.* **2009**, *48*, 7787.
(9) Xia, Y.; Xiong, Y.; Lim, B.; Skrabalak, S. E. *Angew. Chem., Int. Ed.* **2009**, *48*, 60.
(10) Zhou, K.; Li, Y. *Angew. Chem., Int. Ed.* **2012**, *51*, 602.
(11) Somorjai, G. A.; Frei, H.; Park, J. Y. *J. Am. Chem. Soc.* **2009**, *131*, 16589.
(12) Giljohann, D. A.; Seferos, D. S.; Daniel, W. L.; Massich, M. D.; Patel, P. C.; Mirkin, C. A. *Angew. Chem., Int. Ed.* **2010**, *49*, 3280.
(13) Jones, M. R.; Osberg, K. D.; Macfarlane, R. J.; Langille, M. R.; Mirkin, C. A. *Chem. Rev.* **2011**, *111*, 3736.
(14) Jana, N. R.; Gearheart, L.; Murphy, C. J. *Adv. Mater.* **2001**, *13*, 1389.
(15) Sau, T. K.; Murphy, C. J. *J. Am. Chem. Soc.* **2004**, *126*, 8648.
(16) Nikoobakht, B.; El-Sayed, M. A. *Chem. Mater.* **2003**, *15*, 1957.
(17) Kim, D.; Heo, J.; Kim, M.; Lee, Y. W.; Han, S. W. *Chem. Phys. Lett.* **2009**, *468*, 245.
(18) Sohn, K.; Kim, F.; Pradel, K. C.; Wu, J.; Peng, Y.; Zhou, F.; Huang, J. *ACS Nano* **2009**, *3*, 2191.
(19) Xiang, Y.; Wu, X.; Liu, D.; Feng, L.; Zhang, K.; Chu, W.; Zhou, W.; Xie, S. *J. Phys. Chem. C* **2008**, *112*, 3203.
(20) Millstone, J. E.; Métraux, G. S.; Mirkin, C. A. *Adv. Funct. Mater.* **2006**, *16*, 1209.
(21) Millstone, J. E.; Wei, W.; Jones, M. R.; Yoo, H.; Mirkin, C. A. *Nano Lett.* **2008**, *8*, 2526.
(22) Ming, T.; Feng, W.; Tang, Q.; Wang, F.; Sun, L.; Wang, J.; Yan, C. *J. Am. Chem. Soc.* **2009**, *131*, 16350.
(23) Liu, M.; Guyot-Sionnest, P. *J. Phys. Chem. B* **2005**, *109*, 22192.
(24) Zhang, J.; Langille, M. R.; Personick, M. L.; Zhang, K.; Li, S.; Mirkin, C. A. *J. Am. Chem. Soc.* **2010**, *132*, 14012.
(25) Yu, Y.; Zhang, Q.; Lu, X.; Lee, J. Y. *J. Phys. Chem. C* **2010**, *114*, 11119.
(26) Personick, M. L.; Langille, M. R.; Zhang, J.; Mirkin, C. A. *Nano Lett.* **2011**, *11*, 3394.
(27) Garg, N.; Scholl, C.; Mohanty, A.; Jin, R. *Langmuir* **2010**, *26*, 10271.

(28) Chung, P.-J.; Lyu, L.-M.; Huang, M. H. *Chem. Eur. J.* **2011**, *17*, 9746.
(29) Murphy, C. J.; Thompson, L. B.; Chernak, D. J.; Yang, J. A.; Sivapalan, S. T.; Boulos, S. P.; Huang, J.; Alkilany, A. M.; Sisco, P. N. *Curr. Opin. Colloid Interface Sci.* **2011**, *16*, 128.
(30) Navarro, J. R. G.; Manchon, D.; Lerouge, F.; Cottancin, E.; Lermé, J.; Bonnet, C.; Chaput, F.; Mosset, A.; Pellarin, M.; Parola, S. *Nanotechnology* **2012**, *23*, 145707.
(31) Tran, T. T.; Lu, X. *J. Phys. Chem. C* **2011**, *115*, 3638.
(32) Tian, N.; Zhou, Z.-Y.; Sun, S.-G.; Ding, Y.; Wang, Z. L. *Science* **2007**, *316*, 732.
(33) Zhou, Z.-Y.; Tian, N.; Li, J.-T.; Broadwell, I.; Sun, S.-G. *Chem. Soc. Rev.* **2011**, *40*, 4167.
(34) Personick, M. L.; Langille, M. R.; Zhang, J.; Harris, N.; Schatz, G. C.; Mirkin, C. A. *J. Am. Chem. Soc.* **2011**, *133*, 6170.
(35) Langille, M. R.; Personick, M. L.; Zhang, J.; Mirkin, C. A. *J. Am. Chem. Soc.* **2011**, *133*, 10414.
(36) Niu, W.; Zheng, S.; Wang, D.; Liu, X.; Li, H.; Han, S.; Chen, J.; Tang, Z.; Xu, G. *J. Am. Chem. Soc.* **2009**, *131*, 697.
(37) Grzelczak, M.; Pérez-Juste, J.; Mulvaney, P.; Liz-Marzán, L. M. *Chem. Soc. Rev.* **2008**, *37*, 1783.
(38) Bullen, C.; Zijlstra, P.; Bakker, E.; Gu, M.; Raston, C. *Cryst. Growth Des.* **2011**, *11*, 3375.
(39) Murphy, C. J.; Sau, T. K.; Gole, A. M.; Orendorff, C. J.; Gao, J.; Gou, L.; Hunyadi, S. E.; Li, T. *J. Phys. Chem. B* **2005**, *109*, 13857.
(40) Mariscal, M. M.; Oviedo, O. A.; Leiva, E. P. M. *J. Mater. Res.* **2012**, *27*, 1777.
(41) Oviedo, O. A.; Negre, C. F. A.; Mariscal, M. M.; Sánchez, C. G.; Leiva, E. P. M. *Electrochem. Commun.* **2012**, *16*, 1.
(42) Ha, T. H.; Koo, H.-J.; Chung, B. H. *J. Phys. Chem. C* **2007**, *111*, 1123.
(43) Smith, D. K.; Miller, N. R.; Korgel, B. A. *Langmuir* **2009**, *25*, 9518.
(44) Grzelczak, M.; Sánchez-Iglesias, A.; Rodríguez-González, B.; Alvarez-Puebla, R.; Pérez-Juste, J.; Liz-Marzán, L. M. *Adv. Funct. Mater.* **2008**, *18*, 3780.
(45) DuChene, J. S.; Niu, W.; Abendroth, J. M.; Sun, Q.; Zhao, W.; Huo, F.; Wei, W. D. *Chem. Mater.* **2012**, DOI: 10.1021/cm3020397.
(46) Jiao, Z.; Xia, H.; Tao, X. *J. Phys. Chem. C* **2011**, *115*, 7887.
(47) Pérez-Juste, J.; Liz-Marzán, L. M.; Carnie, S.; Chan, D. Y. C.; Mulvaney, P. *Adv. Funct. Mater.* **2004**, *14*, 571.
(48) Rodríguez-Fernández, J.; Pérez-Juste, J.; Mulvaney, P.; Liz-Marzán, L. M. *J. Phys. Chem. B* **2005**, *109*, 14257.
(49) Ma, Y.; Kuang, Q.; Jiang, Z.; Xie, Z.; Huang, R.; Zheng, L. *Angew. Chem., Int. Ed.* **2008**, *47*, 8901.
(50) Wu, H.-L.; Kuo, C.-H.; Huang, M. H. *Langmuir* **2010**, *26*, 12307.
(51) Eguchi, M.; Mitsui, D.; Wu, H.-L.; Sato, R.; Teranishi, T. *Langmuir* **2012**, *28*, 9021.
(52) Bard, A. J.; Parsons, R.; Jordan, J. *Standard Potentials in Aqueous Solution*; Marcel Dekker: New York, 1985.
(53) Brown, L.; Holme, T. *Chemistry for Engineering Students*; Brooks/Cole: Belmont, 2011.
(54) Magnussen, O. M. *Chem. Rev.* **2002**, *102*, 679.
(55) Zhong, J.; Qu, J.; Ye, F.; Wang, C.; Meng, L.; Yang, J. *J. Colloid Interface Sci.* **2011**, *361*, 59.
(56) Suzuki, K.; Hosokawa, K.; Maeda, M. *J. Am. Chem. Soc.* **2009**, *131*, 7518.
(57) Aubin-Tam, M.-E.; Hwang, W.; Hamad-Schifferli, K. *Proc. Natl. Acad. Sci. U.S.A.* **2009**, *106*, 4095.
(58) Wang, Z. L. *J. Phys. Chem. B* **2000**, *104*, 1153.
(59) Vivek, J. P.; Burgess, I. J. *Langmuir* **2012**, *28*, 5031.
(60) Vivek, J. P.; Burgess, I. J. *Langmuir* **2012**, *28*, 5040.
(61) Washio, I.; Xiong, Y.; Yin, Y.; Xia, Y. *Adv. Mater.* **2006**, *18*, 1745.
(62) Zhang, J.; Langille, M. R.; Mirkin, C. A. *J. Am. Chem. Soc.* **2010**, *132*, 12502.
(63) Zhang, J.; Langille, M. R.; Mirkin, C. A. *Nano Lett.* **2011**, *11*, 2495.
(64) Langille, M. R.; Zhang, J.; Mirkin, C. A. *Angew. Chem., Int. Ed.* **2011**, *50*, 3543.
(65) Xue, C.; Mirkin, C. A. *Angew. Chem., Int. Ed.* **2007**, *46*, 2036.
(66) Xue, C.; Millstone, J. E.; Li, S.; Mirkin, C. A. *Angew. Chem., Int. Ed.* **2007**, *46*, 8436.
(67) Xue, C.; Métraux, G. S.; Millstone, J. E.; Mirkin, C. A. *J. Am. Chem. Soc.* **2008**, *130*, 8337.
(68) Michalitsch, R.; Laibinis, P. E. *Angew. Chem., Int. Ed.* **2001**, *40*, 941.
(69) Michalitsch, R.; Palmer, B. J.; Laibinis, P. E. *Langmuir* **2000**, *16*, 6533.
(70) Lee, J.; Oh, I.; Hwang, S.; Kwak, J. *Langmuir* **2002**, *18*, 8025.
(71) Iski, E. V.; El-Kouedi, M.; Calderon, C.; Wang, F.; Bellisario, D. O.; Ye, T.; Sykes, E. C. H. *Electrochim. Acta* **2011**, *56*, 1652.
(72) Herrero, E.; Buller, L. J.; Abruña, H. D. *Chem. Rev.* **2001**, *101*, 1897.
(73) Huang, X.; Tang, S.; Zhang, H.; Zhou, Z.; Zheng, N. *J. Am. Chem. Soc.* **2009**, *131*, 13916.
(74) Yu, T.; Kim, D. Y.; Zhang, H.; Xia, Y. *Angew. Chem., Int. Ed.* **2011**, *50*, 2773.
(75) DeSantis, C. J.; Peverly, A. A.; Peters, D. G.; Skrabalak, S. E. *Nano Lett.* **2011**, *11*, 2164.
(76) Huang, X.; Zhao, Z.; Fan, J.; Tan, Y.; Zheng, N. *J. Am. Chem. Soc.* **2011**, *133*, 4718.
(77) Xia, X.; Zeng, J.; McDearmon, B.; Zheng, Y.; Li, Q.; Xia, Y. *Angew. Chem., Int. Ed.* **2011**, *50*, 12542.
(78) Jin, M.; Zhang, H.; Xie, Z.; Xia, Y. *Angew. Chem., Int. Ed.* **2011**, *50*, 7850.
(79) Carbó-Argibay, E.; Rodríguez-González, B.; Gómez-Graña, S.; Guerrero-Martínez, A.; Pastoriza-Santos, I.; Pérez-Juste, J.; Liz-Marzán, L. M. *Angew. Chem., Int. Ed.* **2010**, *49*, 9397.
(80) Katz-Boon, H.; Rossouw, C. J.; Weyland, M.; Funston, A. M.; Mulvaney, P.; Etheridge, J. *Nano Lett.* **2010**, *11*, 273.
(81) Nehl, C. L.; Liao, H.; Hafner, J. H. *Nano Lett.* **2006**, *6*, 683.
(82) Kumar, P. S.; Pastoriza-Santos, I.; Rodríguez-González, B.; García de Abajo, F. J.; Liz-Marzán, L. M. *Nanotechnology* **2008**, *19*, 015606.
(83) Zhang, H.; Li, W.; Jin, M.; Zeng, J.; Yu, T.; Yang, D.; Xia, Y. *Nano Lett.* **2011**, *11*, 898.